NASA/TM–2012-217336

Simplified Models for the Study of Postbuckled Hat-Stiffened Composite Panels

Riccardo Vescovini
Politecnico di Milano, Milano, Italy

Carlos G. Dávila
Langley Research Center, Hampton, Virginia

Chiara Bisagni
Politecnico di Milano, Milano, Italy

February 2012

NASA STI Program . . . in Profile

Since its founding, NASA has been dedicated to the advancement of aeronautics and space science. The NASA scientific and technical information (STI) program plays a key part in helping NASA maintain this important role.

The NASA STI program operates under the auspices of the Agency Chief Information Officer. It collects, organizes, provides for archiving, and disseminates NASA's STI. The NASA STI program provides access to the NASA Aeronautics and Space Database and its public interface, the NASA Technical Report Server, thus providing one of the largest collections of aeronautical and space science STI in the world. Results are published in both non-NASA channels and by NASA in the NASA STI Report Series, which includes the following report types:

- TECHNICAL PUBLICATION. Reports of completed research or a major significant phase of research that present the results of NASA programs and include extensive data or theoretical analysis. Includes compilations of significant scientific and technical data and information deemed to be of continuing reference value. NASA counterpart of peer-reviewed formal professional papers, but having less stringent limitations on manuscript length and extent of graphic presentations.

- TECHNICAL MEMORANDUM. Scientific and technical findings that are preliminary or of specialized interest, e.g., quick release reports, working papers, and bibliographies that contain minimal annotation. Does not contain extensive analysis.

- CONTRACTOR REPORT. Scientific and technical findings by NASA-sponsored contractors and grantees.

- CONFERENCE PUBLICATION. Collected papers from scientific and technical conferences, symposia, seminars, or other meetings sponsored or co-sponsored by NASA.

- SPECIAL PUBLICATION. Scientific, technical, or historical information from NASA programs, projects, and missions, often concerned with subjects having substantial public interest.

- TECHNICAL TRANSLATION. English-language translations of foreign scientific and technical material pertinent to NASA's mission.

Specialized services also include creating custom thesauri, building customized databases, and organizing and publishing research results.

For more information about the NASA STI program, see the following:

- Access the NASA STI program home page at *http://www.sti.nasa.gov*

- E-mail your question via the Internet to help@sti.nasa.gov

- Fax your question to the NASA STI Help Desk at 443-757-5803

- Phone the NASA STI Help Desk at 443-757-5802

- Write to:
  NASA STI Help Desk
  NASA Center for AeroSpace Information
  7115 Standard Drive
  Hanover, MD 21076-1320

NASA/TM–2012-217336

Simplified Models for the Study of Postbuckled Hat-Stiffened Composite Panels

Riccardo Vescovini
Politecnico di Milano, Milano, Italy

Carlos G. Dávila
Langley Research Center, Hampton, Virginia

Chiara Bisagni
Politecnico di Milano, Milano, Italy

National Aeronautics and
Space Administration

Langley Research Center
Hampton, Virginia 23681-2199

February 2012

Available from:

NASA Center for AeroSpace Information
7115 Standard Drive
Hanover, MD 21076-1320
443-757-5802

Simplified Models for the Study of Postbuckled Hat-Stiffened Composite Panels

R. Vescovini[1], C.G. Dávila[2], C. Bisagni[1]

[1]*Politecnico di Milano, Department of Aerospace Engineering, Milano, Italy*
[2]*NASA Langley Research Center, Hampton, Virginia, USA*

Abstract

The postbuckling response and failure of multistringer stiffened panels is analyzed using models with three levels of approximation. The first model uses a relatively coarse mesh to capture the global postbuckling response of a five-stringer panel. The second model can predict the nonlinear response as well as the debonding and crippling failure mechanisms in a single stringer compression specimen (SSCS). The third model consists of a simplified version of the SSCS that is designed to minimize the computational effort. The simplified model is well-suited to perform sensitivity analyses for studying the phenomena that lead to structural collapse. In particular, the simplified model is used to obtain a deeper understanding of the role played by geometric and material modeling parameters such as mesh size, interlaminar strength, fracture toughness, and fracture mode mixity. Finally, a global/local damage analysis method is proposed in which a detailed local model is used to scan the global model to identify the locations that are most critical for damage tolerance.

I. Introduction

Composite stiffened panels are commonly used as components for the construction of aerospace structures. In most cases, stiffened panels can operate far beyond the buckling load and their collapse is observed deep into the postbuckling range. For this reason, the ability to predict the collapse load and the mechanisms involved in the failure is a crucial point for the damage tolerance assessment and the rational design of these structures.

Experiments conducted on stiffened panels[1,2] and closed-box configurations[3,4] represent a useful mean to gather insight into the complex nonlinear response governing the collapse. However, the high manufacturing and testing costs associated with multistringer panels strongly limits the possibility of

performing extensive experimental explorations. For this reason, the availability of analytical and numerical tools is fundamental to further investigate the collapse response of postbuckled composite panels. In recent years, several strategies have been developed for the study of the damage onset and propagation, including skin/stringer delaminations. An analytical approach was proposed by Taki and Kitagawa[5] to predict the failure load of composite stiffened panels under shear load. The methodology is based on a strip analysis to determine the loading conditions that would cause a disbond of the stringer from the skin.

More recently, Cosentino and Weaver[6] proposed a nonlinear approach to predict crack initiation in composite stiffened panels. The approach is based on the use of two linked analytical models. The first model adopts a nonlinear formulation that provides the stress and displacement fields throughout the domain. The second model predicts crack initiation using a closed-form linear elastic fracture mechanics solution. Despite their efficiency, analytical and semi-analytical methods can be developed only by introducing a number of simplifying assumptions. In general, the failure of postbuckled panels involves several nonlinear mechanisms, including geometric as well as material nonlinearities that cannot be captured properly by analytical models. Finally, the inadequacy of analytical models can be exacerbated by the existence of different failure mechanisms, including interlaminar and intralaminar damage phenomena.

Alternatively, the finite element method can be used to predict arbitrary complex postbuckling responses, and different analysis tools such as progressive failure methods[7,8], continuum damage models[9,10], virtual crack closure technique[11], cohesive elements[12,13] and X-FEM[14] are available to study different aspects of the failure process. However, the computational requirements associated with failure analysis often render these methods unsuited to study even moderately large structural components. For this reason, different strategies have been proposed to reduce the computational cost.

Orifici et al.[15] developed a computationally efficient two-step global/local approach to identify interlaminar damage initiation. The approach adopts a strength-based criterion, which is applied to a model of the skin–stringer interface at a ply-level mesh refinement. A global/local approach has been proposed by Bertolini et al.[16] to assess the response of stiffened panels under compression and shear. In this case, the VCCT technique is used to determine the energy release rates and the Benzeggagh–Kenane mixed-mode fracture criterion[17] is applied.

The goal of the present work is to develop simplified and computationally efficient models to predict the response and collapse of a stiffened panel and to perform sensitivity studies to gain deeper understanding of the phenomena that lead to local and global collapse and to optimize the finite element models used in the calculations. The optimized models at several scales of complexity are also combined in a global/local strategy for the collapse analysis of a multistringer panel.

II. Modeling hat-stiffened panels with three levels of complexity

In a previous numerical/experimental investigation[18], the authors proposed the use of a Single Stringer Compression Specimen (SSCS) to study the response and the failure of a multistringer panel loaded in compression. The configuration of the SSCS is shown in Figure 1(a), and a picture of a compression test is shown in Figure 1(b).

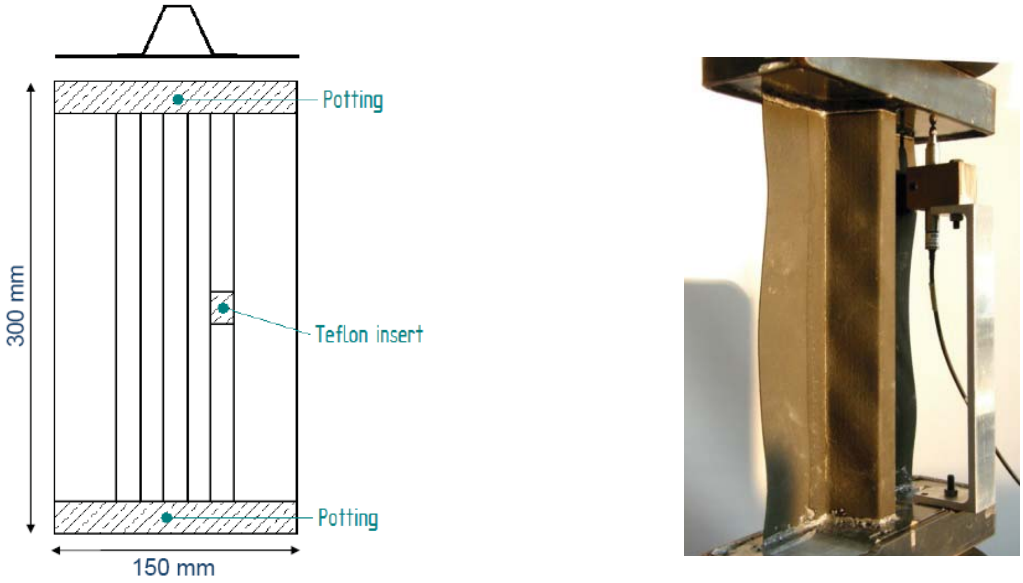

Figure 1. Single Stringer Compression Specimen (SSCS): (a) configuration and dimensions, (b) compression test.

The SSCS represents an intermediate level of complexity between coupon-level specimens and structural components while exhibiting most of the challenges that characterize the assessment of the damage behavior of a more complex configuration such as a multistringer panel. Advantages exist from the experimental point of view, due to low manufacturing and testing costs, and from the numerical point of view, due to the possibility of realizing refined meshes. The authors performed Abaqus[19] finite element analyses with a user defined continuum damage model[9,10] for the study of intralaminar damage mechanisms, and cohesive elements[7,13] to account for delaminations between the skin and the stringer. Despite the small size of the SSCS and the efforts devoted to maximize the computational efficiency by combining quasi-static and implicit steps, the numerical study of the failure of a SSCS still requires several days of analysis. It is clear that such lengthy analyses render the use of this approach for sensitivity analyses or for the analysis of multistringer panels intractable, and that an alternative methodology is necessary.

The present study presents the results of an investigation into the collapse response of a multistringer composite panel using models characterized by the three levels of structural complexity illustrated in Figure 2.

In order of decreasing complexity, the models are the complete multistringer panel, the single stringer compression specimen, and the simplified model, shown in Figures 2(a)-(c). The analyses in the following sections are conducted using Abaqus/Std[19] with an implicit dynamic solution procedure. The models use four-noded S4R shell elements. The SSCS and simplified models also use cohesive elements between the skin and the stringer flange to represent skin/stringer separation.

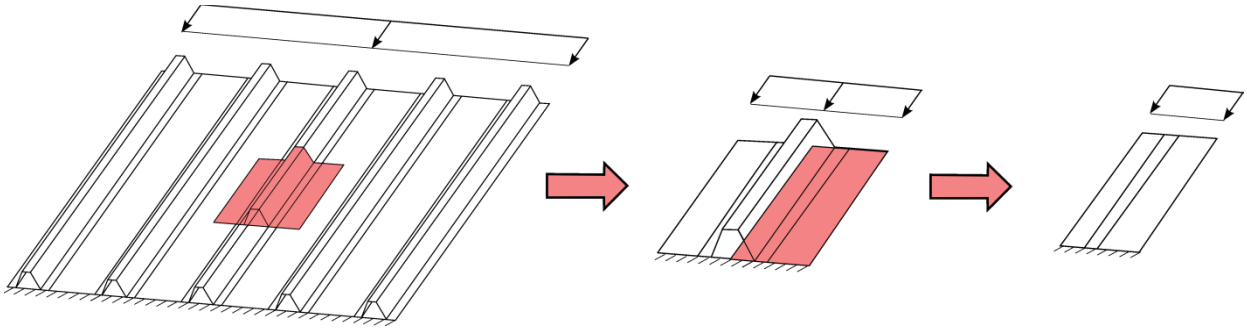

Figure 2. Structural models: (a) multistringer panel, (b) SSCS, (c) simplified model.

A. Multistringer panel

The multistringer panel illustrated in Figure 2(a) has a length of 720 *mm* and a width of 680 *mm*. The panel is stiffened longitudinally by five hat-stringers. The height of the stringers is 30 *mm*, the width of the crown top is 15 *mm*, while the web is at an angle of 25° with the normal to the skin. The stringers are co-cured to the skin along two 15 *mm*-wide flanges. Both the skin and the stringers are made from IM7/8552 graphite-epoxy material. The skin consists of 8-ply quasi-isotropic laminate with stacking sequence of $[45°/90°/-45°/0°]_s$. The stringers are composed of 7-ply laminate with a symmetric stacking sequence of [-45°/0°/45°/0°/45°/0°/-45°].

The material elastic and interlaminar properties[20] are summarized in Tables 1 and 2, respectively.

Table 1. Engineering properties – IM7/8552.

E_{11} (*MPa*)	E_{22}(*MPa*)	G_{12}(*MPa*)	ν_{12}	α_1 (*1/°C*)	α_2 (*1/°C*)
150000	9080	5290	0.32	-5.5E-6	25.8E-6

Table 2. Interlaminar properties – IM7/8552.

GI_c (*N/mm*)	GII_c (*N/mm*)	σ_{zz} (*MPa*)	σ_{xz} (*MPa*)
0.277	0.788	50	100

The postbuckling quasi-static response of this five stringer panel can be obtained relatively quickly as long as the material nonlinearities are not taken into account. However, the mesh requirements needed for predicting intralaminar and interlaminar damage, together with the rather large dimensions of the panel, render the prediction of damage at this scale computationally impractical.

B. Single Stringer Compression Specimen (SSCS)

The Single Stringer Compression Specimen (SSCS) considered in this study is illustrated in Figure 2(b). The specimen is composed of one stringer, and extends transversally from half bay to half bay, for a total width of 150 *mm*. This structural component represents a small portion of the multistringer panel and was designed to have similar response characteristics as the corresponding multistringer panel. Through parametric studies, it was found that a SSC specimen length of 240 *mm* resulted in a stress distribution that is similar to that observed in the multistringer panel[18]. The reduced dimensions of this specimen

diminish the manufacturing and testing costs and permit the use of sufficiently detailed finite element meshes to study the interlaminar and intralaminar damage mechanisms.
The SSCS model can be used to assess the damage tolerance of the multistringer panel, as the similarity of the stress distributions and of the buckled patterns determines analogous failure mechanisms. Nevertheless, the analysis of the SSCS model with damage requires several days of computational time[18], so that it is inadequate to perform the sensitivity studies necessary to fully understand the collapse response of the panel or to evaluate the effect of different modeling parameters on the analysis results. Consequently, a further level of approximation is introduced in the next section.

C. Simplified model

A simplified model developed to reduce the computational requirement for analysis is schematically illustrated in Figure 2(c). As is explained in the following section, the model is obtained from an examination of the response of the SSCS by removing the stringer from the SSCS and by using symmetry along the stringer mid-plane. The smaller dimensions and the reduced number of degrees of freedom make the model well-suited to perform sensitivity analyses with a relatively small computational effort. The simplified model is also useful to gain knowledge about the effects of the different modeling parameters on the analysis results and to define the properties of the SSCS model used in the context of the global/local procedure.

III. Development of a simplified model

The structural response of the SSC specimen is briefly described to highlight the most important aspects leading to the development of a simplified structural model. The panel is loaded with an end shortening displacement, as illustrated in Figure 2. The ending tabs of the specimens are simulated by constraining the translational degrees of freedom of the corresponding nodes, while the longitudinal edges are free.
In the initial loading phase, corresponding to the prebuckling conditions, the SSCS exhibits a linear response. The first buckling is observed at a load of about 10 *kN*, and mainly regards the instability of the skin, which buckles in three half-waves. No buckling deformations are observed on the stringer, as can be observed in Figure 3(a). The drop of stiffness in the initial postbuckling range is consequently due to the loss of stiffness of the skin only. As the load is increased further, the deflections on the skin increase in magnitude and, as the load redistributes, the stringer carries an increasing portion of the applied load. After an applied load of approximately 25 *kN*, nonlinear deformations of the stringer web can be observed, as shown in Figure 3(b). The magnitude of the displacements increases progressively with the applied load.

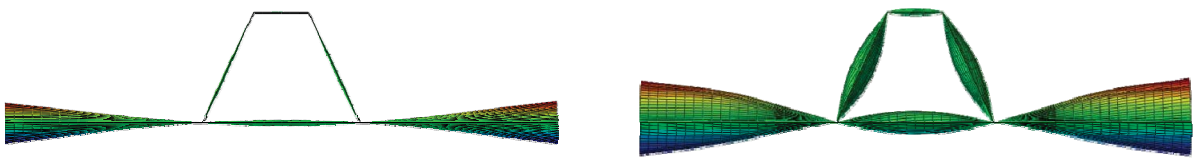

(a) **(b)**

Figure 3. Nonlinear deformation of the SSCS (end view): (a) at first buckling, (b) after buckling of the stringer web.

An investigation of the response and failure of the SSCS model indicates that the delamination onset is governed by the postbuckling deformation on the portion of skin under the stringer. This deformation under the stringer is characterized by three half-waves along the longitudinal direction, as shown in Figure 4(a). At a load of approximately 37 *kN*, a mode transition is observed in which the middle buckle divides into two smaller half-waves, as can be seen in Figure 4(b). This postbuckled configuration, which is composed of four half-waves, causes an internal stress redistribution that promotes the skin/stringer debonding. With a small increase in the load, the most severely loaded cohesive element reaches a fully damaged state, which triggers an unstable propagation of the delamination. As Figure 4(c) indicates, the delamination initiates from the inner edge of the stringer flange. The delamination is soon followed by a large-scale detachment of the skin from the stringer and crippling fracture of the stringer.

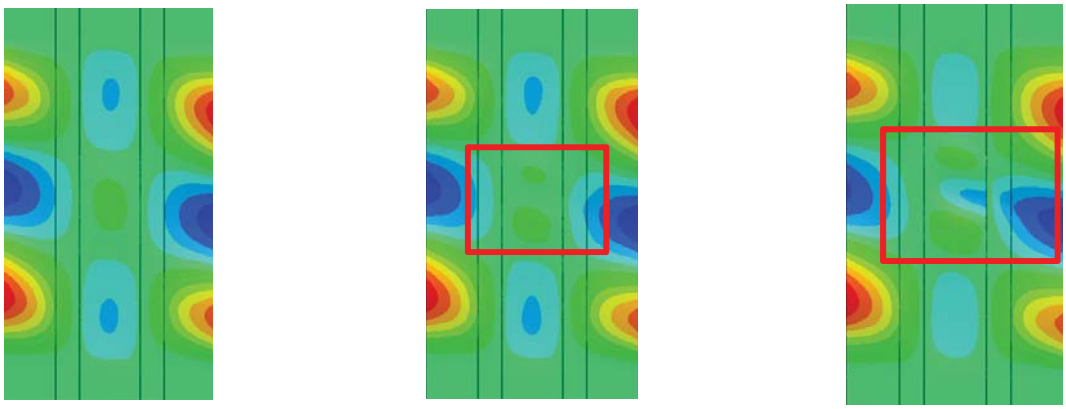

(a) **(b)** **(c)**

Figure 4. Out-of-plane-deflections (view without stringer): (a) initial postbuckling at 35 *kN*, (b) mode jumping at 37 *kN*, (c) delamination onset at 39 *kN*.

Based on these observations of the structural response of the SSCS, a simplified structural model that can reproduce the collapse response with as few degrees of freedom as possible was developed. In particular, the model captures the correct initial skin buckling deformation mode, the mode change under the stringer, and the skin/stringer delamination.

The computational efficiency of the simplified model is a result of modeling only half of the structure and substituting the stringer by means of nodal constraints. In addition, intralaminar damage is not represented and the residual thermal strains are neglected. The SSCS model and the associated simplified model are shown in Figure 5.

As previously observed, the postbuckling deformation of the SSCS is nearly symmetric along the stringer. Using the reference frame in Figure 5(b), symmetry can be imposed by setting to zero the rotations around the *x-axis* and the translation along the transverse *y-axis*. The imposition of symmetry introduces a level of approximation due to the fact that the skin is layered with a flexurally anisotropic lay-up. The resulting coupling between bending and twisting causes skew in the buckling half-waves that are inconsistent with symmetry conditions. There is also additional error when modeling a SSCS with an embedded delamination. In the SSCS tested, Teflon is placed under one of the stringer flanges to create an embedded delamination. The simplified model represents embedded delaminations under both flanges.

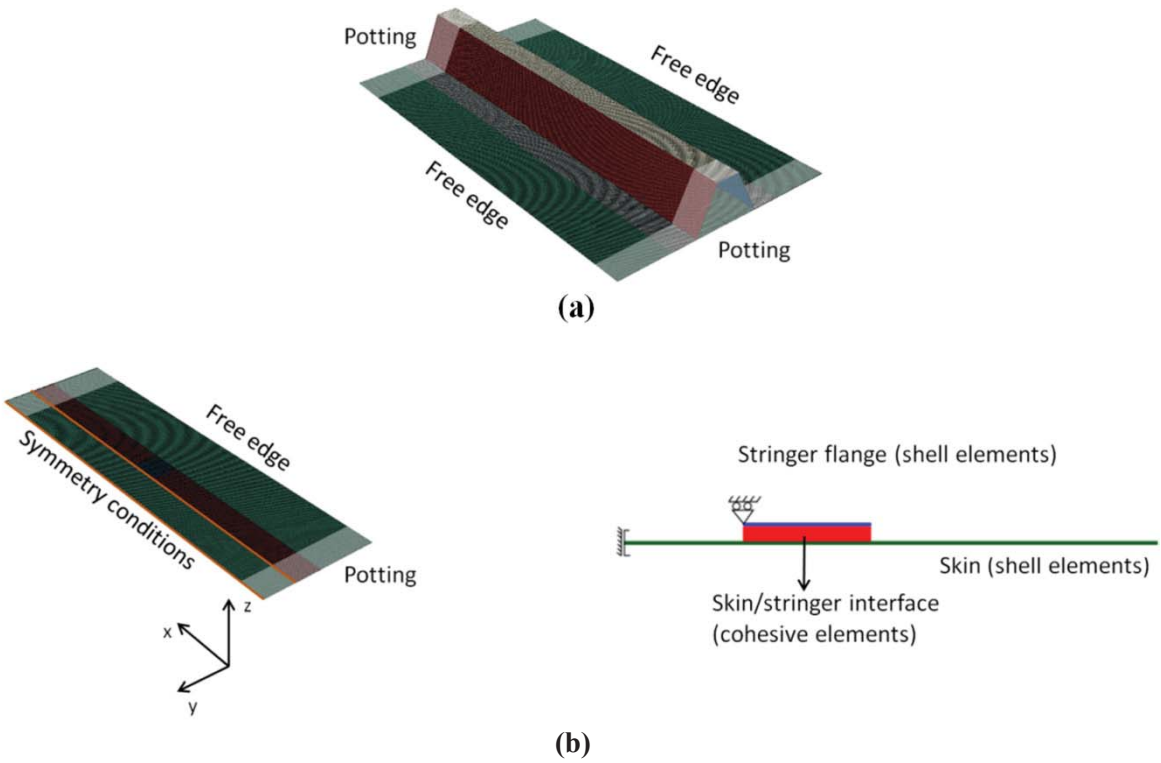

Figure 5. Finite element models and boundary conditions: (a) SSC specimen, (b) simplified model without stringer.

The second observation that is exploited to define a simplified model is that the deformation of the stringer does not contribute appreciably to the process of delamination. The mode transition of the portion of skin under the stringer is driven by the deflections of the outer skin, and the stringer does not need to be modeled explicitly to reproduce the collapse response of the structure. Consequently, in the simplified model the stringer is removed and replaced by simply-supported boundary conditions, as illustrated in Figure 5(b). The model relies on the assumption that the stringer is stiff enough to furnish an ideal constraint to the out-of-plane displacements of the skin. The rotation along the longitudinal axis is free, and consequently no bending moments are exchanged between the stringer and the skin.

As in the SSCS, the simplified model uses cohesive elements to represent the debonding of the stringer flange. However, intralaminar damage of the matrix and fiber, which in the SSCS model was captured using a continuum damage model, is not considered in the simplified model. Intralaminar damage can be neglected because the SSCS analyses indicates that the collapse and crippling of the stringer is caused by the detachment of the stringer. By limiting material nonlinearities to the cohesive layer under one flange the convergence rate of the load incrementation procedure improves dramatically.

Finally, an additional decrease in the computational cost of the simplified model is achieved by neglecting the residual thermal strains that result from the high-temperature cure cycle used in the manufacturing process.

IV. Comparison between SSCS and simplified model

The ability of the simplified structural model to reproduce the sequence of events is assessed by comparing the results obtained with those from the SSCS model. A mesh size of 1.0 *mm* is chosen for both models. The total number of elements and degrees of freedom of the two models is summarized in TTable 3, where it can be observed that the number of degrees of freedom of the simplified model is approximately a third of that for the SSCS model.

Table 3: Number of elements and degrees of freedom of the SSCS and the simplified model.

	SSCS	Simplified model
Number of elements	84,000	30,520
D.o.f.	451,848	158,484

The postbuckling deformations of the SSCS and the simplified model are shown in Figure 6 and the ability of the simplified model to predict initial buckling, mode jumping of the skin under the stringer and delamination onset is evaluated. Figures 6(a) and 6(b) indicate that the first instability, characterized by skin buckling in three half-waves, is properly represented by the simplified model. The most pronounced deflections are found along the edges of the skin, and minor deflections are observed on the stringer. Smaller half-waves are also visible in the skin under the stringer. When the load is increased, the two models present a similar transition of the postbuckling deformation under the stringer, as highlighted in Figures 6(c) and 6(d). In particular, both the SSC specimen and the simplified model display the mode jumping of the mid-buckle, which determines the redistribution of the internal forces and leads to the delamination between the skin and the stringer flange. It should be noted that the stringer is removed in Figures 6(c) and 6(e) for visualization purposes only.

The force–displacement results for the SSCS and the simplified model are compared in Figures 7(a) and 7(b). To account for the stiffness of the stringer, which is not present in the simplified model, the fraction of load carried by the stringer is added *ex post* as:

$$P_{total} = P_{fem} + \frac{EA}{a}U \tag{1}$$

where P_{total} is the total load, P_{fem} is the fraction of load carried by the skin and the stringer flange and available from the finite element analysis, EA is the stringer axial stiffness, a is the panel length and U is the applied displacement. The results in Figure 7(a) correspond to a pristine specimen, while the results in Figure 7(b) correspond to a specimen with a 20-*mm* pre-existing delamination between the skin and the stringer. In the SSCS model, the pre-existing defect is placed under the middle of one of the stringer flanges, as shown in Figure 1(a). Since the simplified model relies on symmetry conditions, it represents a specimen with pre-existing defects under both stringer flanges.

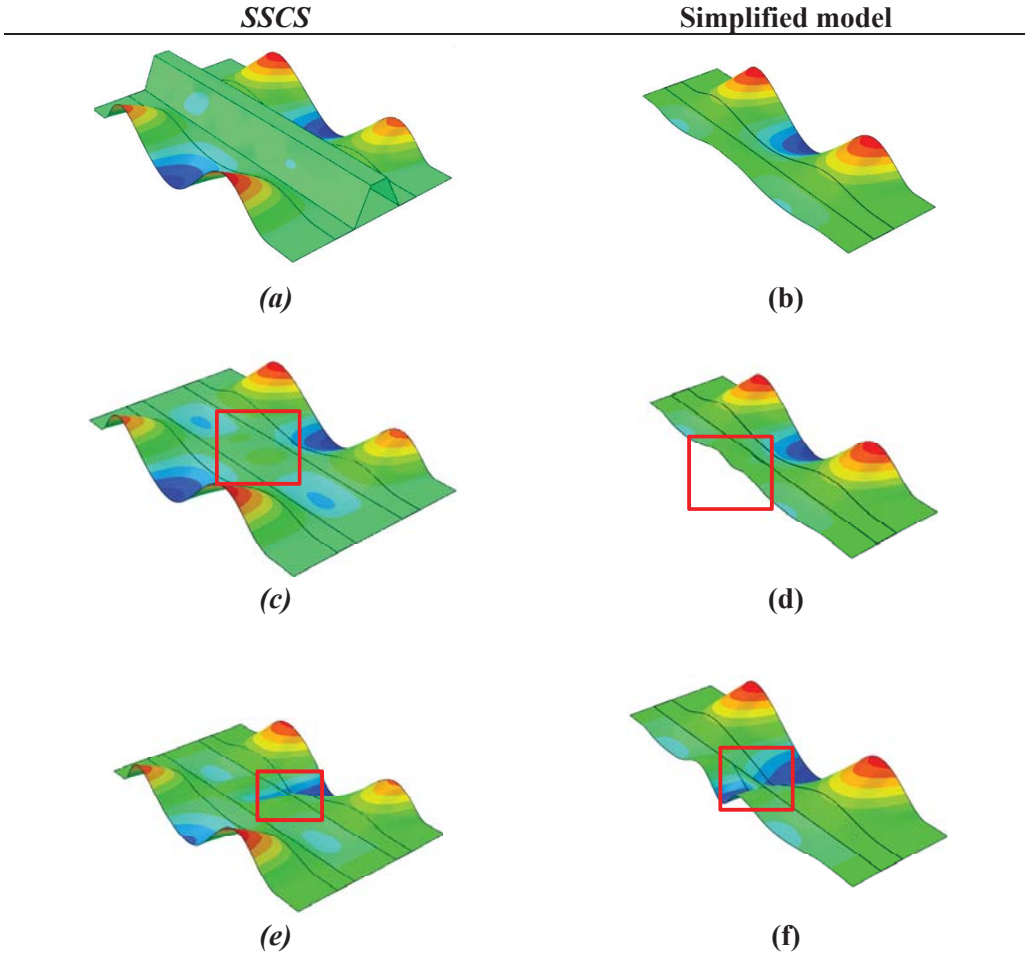

Figure 6. Comparison of postbuckling deflections:
(a)-(b) buckling, (c)-(d) mode jumping and delamination onset, (e)-(f) delamination after collapse.

The results of Figure 7 reveal almost identical prebuckling and postbuckling stiffnesses. Indeed, the postbuckling response of the SSCS specimen is governed by the skin buckling, and no significant errors are introduced by removing the stringer from the model.

The collapse load obtained with the simplified model is underestimated by 8% and 15% in the case of nominally pristine and pre-damaged panels, respectively.

The results illustrate the ability of the simplified model to reproduce the structural response and failure of the SSC specimen and they validate the use of symmetry boundary conditions and the representation of the stringer as a simple support boundary condition. The advantage of the simplified model becomes clear when considering that it requires less than 3 hours of computational time on a quad-core workstation, compared to 7 days for the SSCS model.

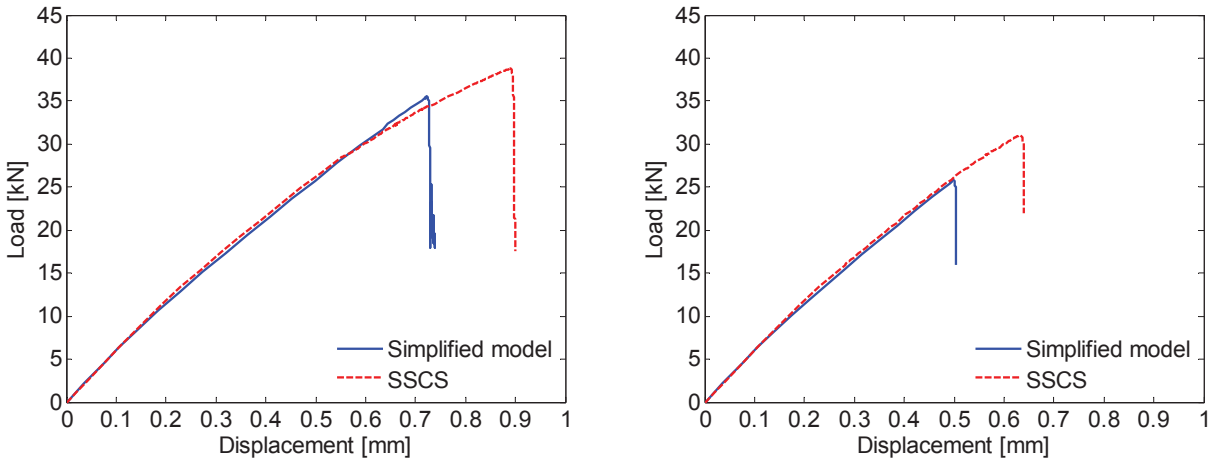

Figure 7. Comparison of force-displacement curves: (a) nominally pristine panel, (b) pre-damaged panel.

V. Simplified model for parameter evaluation

The simplified model is an effective tool for performing sensitivity studies to investigate the effect of the various modeling parameters. These studies provide deeper insight into the structural response of postbuckled hat-stiffened panels, and furnish information that is useful for optimizing the models. In the following sections, the effects of mesh size, interlaminar strength, fracture toughness, and mode mixity are examined.

A. Determination of mesh size requirements

The selection of the optimal mesh size is one of the most important factors in determining the computational requirements of an analysis. Cohesive elements often dictate a model's mesh requirements since the cohesive elements must be small enough to capture the gradients in the process zone. Therefore, cohesive elements are normally much smaller than the elements needed to represent structural response. The length of process zone, l_p, can be estimated as[21]:

$$l_p = \gamma \frac{E G_c}{\sigma_{zz}^2} \tag{2}$$

where $\gamma \approx 0.884$ is a nondimensional parameter, E is approximately equal to the Young's modulus in the direction transverse to the fibers, G_c is the mode I fracture toughness and σ_{zz} is the interlaminar peel strength. For the interface properties shown in Table 2, the process zone length is $l_p \approx 0.85$ *mm*. Consequently, it can be expected that a mesh size smaller than 0.85 *mm* is necessary to represent delamination. This assumption is evaluated by conducting the following analyses.

The results of analyses obtained using mesh sizes equal to 0.5 *mm* and 1.0 *mm* are presented in Figures 8(a) and 8(b). The finer mesh of Figure 8(a) is able to predict the load drop due to initiation and propagation of a delamination between the skin and the stringer flange. The final point of the simulation

corresponds to a delamination that has propagated across the entire width of the stringer flange. The predicted collapse load is 37 *kN*.

The analysis of a model using a 1.0 *mm* element size terminates due to convergence issues at an applied load of about 38 *kN*. The predicted force-displacement result shown in Figure 8(b) does not display a load drop due to delamination. Consequently, a 1.0 *mm* mesh is too coarse to predict the delamination.

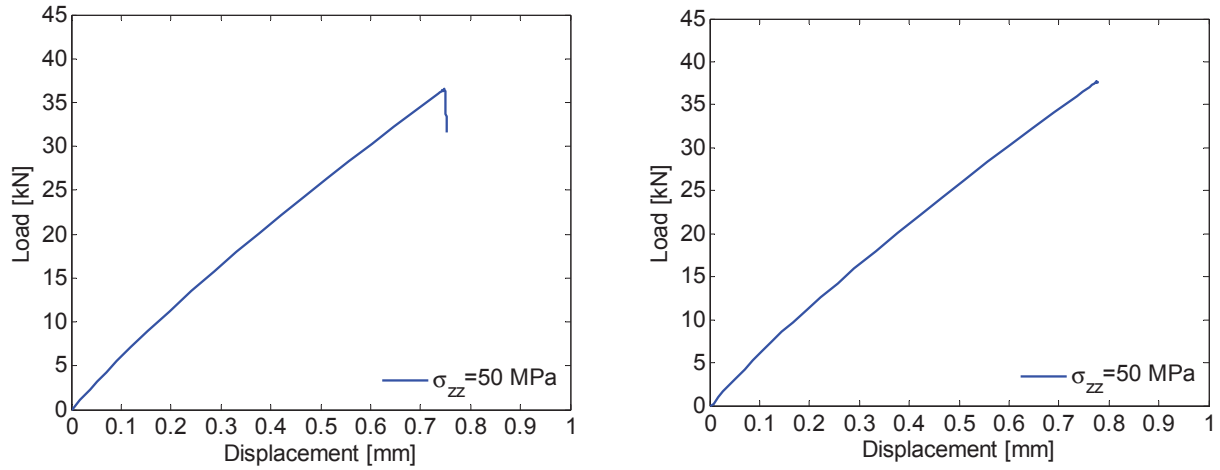

Figure 8. Mesh size: (a) 0.5 x 0.5 *mm*, (b) 1.0 x 1.0 *mm*.

B. Interlaminar strength

Equation 2 shows that the length of the process zone, and consequently the maximum size of the element, can be increased by decreasing the interlaminar strength. Clearly, the value cannot be arbitrarily modified because it represents a mechanical property of the material. However, it is reasonable to reduce the interlaminar strength if the collapse response of the structure is not significantly affected by this value. The investigation of this aspect is the object of the next section.

The study of the panel response for different values of interlaminar strength has two purposes. The first goal is to verify the possibility of enlarging the process zone with a reduction of σ_{zz} without affecting the predicted collapse load. If this is the case, the maximum size of the element can be increased, and a coarser mesh can be used. The second goal is to evaluate how much the collapse of the panel is influenced by the interlaminar strength.

The force-displacement curve of Figure 9 reports the comparison between two different configurations. The first configuration is the nominal configuration and is characterized by a mesh size of 0.5 *mm* and interlaminar strength σ_{zz} equal to 50 *MPa*. The second configuration considers a reduced value of interlaminar strength equal to 25 *MPa*. According to Eq. (2), a reduction of the interlaminar strength determines an increase of the length of the process zone. For this reason, the second configuration is realized with a coarser mesh size of 1.0 *mm*.

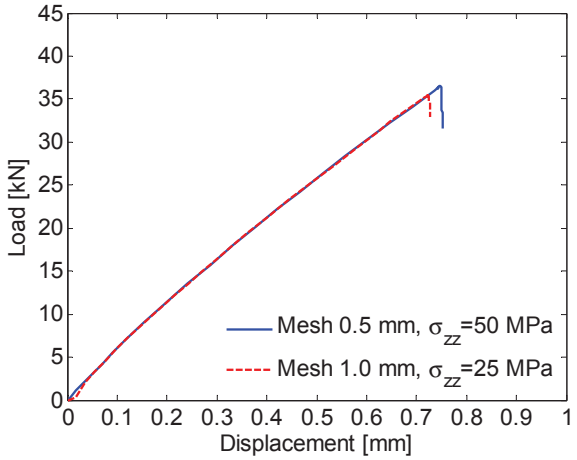

Figure 9. Force-displacement curve panels with different interlaminar strengths and mesh sizes.

It can be observed from Figure 9 that the collapse load of the nominal configuration is 36.5 *kN*, whereas the one obtained with the coarser mesh is 35.5 *kN*. The drawback associated to the use of the 1.0 *mm* mesh is that the collapse load is underestimated. However, the percent difference between the two results is below 3%. It is then retained that a mesh size of 1.0 *mm* with an interlaminar strength equal to 25 *MPa* represents a good compromise in terms of accuracy of the predicted collapse load and required analysis time. For this reason, these values will be used in the next sections to perform further parametric studies.

C. Fracture toughness and R-curve effect

The opening Mode I interlaminar fracture toughness, GI_c, measured with standards such as the ASTM-D5528 represent the GI_c for crack initiation. Most fracture processes exhibits a resistance-type behavior (R-curve), which consists of an initial monotonic increase in GI_c, followed by propagation at a stabilized value of GI_c. In double cantilever beam specimens composed of unidirectional material, the increase in fracture toughness with crack length is mostly attributable to fiber bridging. An even larger R-curve effect is obtained when measuring the fracture toughness at interfaces between different fiber orientations, such as is the case between the skin and the stiffener. In these laminates, the increase in fracture toughness is likely due to the formation of somewhat tortuous delamination paths, which could include jumping of the delaminations to different interfaces in the laminate. For example, Shön et al.[22] determined that the fracture toughness between 45° plies increases from about 0.22 *N/mm* to about 0.9 *N/mm* after 15 *mm* of propagation. Pereira and de Morais[23] measured the fracture toughness between a 0°-ply and plies oriented at 0°, 67.5° and 90°, and found that for 0°/0° interfaces GI_c increases from 0.3 *N/mm* to 0.65 *N/mm* after approximately 35 *mm* of propagation, while the toughness of other interfaces tested exhibits increases from 0.35 *N/mm* to 1.2 *N/mm* in 30 *mm* of propagation.

Given the importance of GI_c in the analysis of the SSCS and the uncertainty in the R-curve effect associated with skin/stringer debonding, analyses were conducted to examine the effect of an R-curve on the predicted collapse load. The analyses were performed on nominally pristine as well as specimens with an implanted 20-*mm* delamination between the skin and the stringer. For each case, three analyses were conducted. The first set of analyses considers the nominal, i.e., initiation value of GI_c=0.277 *N/mm*, which was shown in Table 2. The second set uses GI_c=1.00 *N/mm*, which approximates the value for steady state propagation described in the previous paragraph. The third set considers an R-curve that initiates at

GI_c=0.277 *N/mm* and increases to 1.00 *N/mm* in 15 *mm*. The R-curve simulation is conducted by means of a superposition of two cohesive laws[21] in which the first law represents the crack initiation value of 0.277 *N/mm*, which is denoted by G_1, and a second law that represents the crack bridging effects and accounts for the remaining 0.723 *N/mm* of fracture toughness, which is denoted by G_2. The superposition approach proposed in Ref.[21] provides a means to determine the strengths σ_1 and σ_2 for the two cohesive laws :

$$\sigma_1 = \sigma_c \left[1 - \frac{2}{3}\left(1 - \frac{G_1}{G_1 + G_2}\right)\frac{l_c}{l_{ss}}\right] \qquad (3)$$

$$\sigma_2 = \sigma_c - \sigma_1$$

For a steady-state length of propagation l_{ss}=15 *mm,* l_c=2.4 *mm,* and σ_c=25 *MPa*, Eq. (3) gives σ_1=23 *MPa*, σ_2=2 *MPa*.

The force-displacement curves predicted by the six analyses are shown in Figures 10(a) and 10(b). The response of a nominally pristine panel is shown in Figure 10(a), whereas the results for the panel with a pre-existing delamination is shown in Figure 10(b). The three models are realized with a 1.0 *mm* mesh and interlaminar strength of 25 *MPa*.

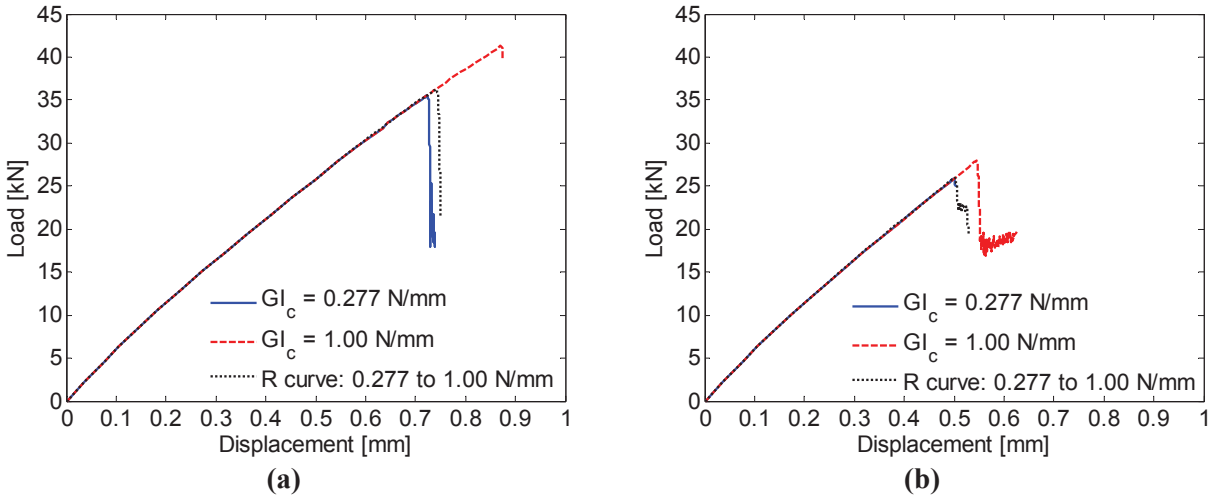

Figure 10. Effect of fracture toughness on pristine panel and panel with initial delamination: (a) nominally pristine panel, (b) panel with initial delamination.

The results indicate that increasing the value of GI_c from its initiation value of 0.277 *N/mm* to a steady-state value of 1.00 *N/mm* causes an increase in the collapse load of 14% in the case of the pristine panel, and 7.5% for the panel with a pre-existing delamination. These relatively modest increases indicate that the collapse of the panel is governed more by the postbuckling deformation mode than by the fracture toughness. The results also indicate that the incorporation of an R-curve effect by cohesive superposition has a negligible effect on the collapse load of both panels when compared to the predictions made with the initiation value of the fracture toughness.

D. Summary of the sensitivity analyses

The sensitivity studies performed with the simplified model provide a deeper understanding into the response and collapse of postbuckled hat-stiffened panels. These analyses also help to evaluate improvements in the model for greater computational efficiency. It was found that a mesh size of 1.0 *mm* can be used if interlaminar strength is reduced from the nominal value of 50 *MPa* to 25 *MPa*. Indeed, a reduction of the interlaminar strength does not affect the collapse load, which is reduced by 3%. It was also found that the collapse is geometrically driven and, consequently, that the interlaminar strength and the fracture toughness have a small influence on the collapse load.

VI. Simplified model for structural design

In a design environment, computational efficiency and modeling simplicity are paramount. The present simplified model is useful for design purposes because it requires a short analysis time and because it is parametric, i.e., all of its dimensions, mesh density, material parameters and loading conditions are defined as variable parameters in the input, so the modeling effort required for analyzing multiple configurations is minimal. The ability of the simplified model to provide useful design information with modest modeling efforts and computational cost is illustrated in the following two studies. Firstly, the model is used to assess the effect of different sizes of pre-existing defects on the collapse load of the structure. Secondly, the model is used to evaluate a stringer design concept for improved strength.

A. Evaluation of effects of bondline defects

The ability of stiffened composite structures to operate deep into postbuckling is limited by the potential of presence of defects that could cause premature detachment of the stringer. In the present sudy, the effect of the size of a pre-existing bondline defect between the stringer and skin is investigated. These defects are introduced in the model at the center of the specimen, under the stringer flange. Defect sizes varying between 0 and 60 *mm* are considered. The results are summarized in Figure 11. The mesh size is fixed to 1.0 *mm*, the interlaminar strength is 25 *MPa*, and the fracture toughness in mode I is 0.277 *N/mm*. The defect is modeled with a layer of cohesive elements with reduced properties consisting of an interlaminar strength of 2.5 *MPa* and a mode I fracture toughness of 0.277e-2 *N/mm*. These properties represent the extremely low adhesion of the Teflon film and the presence of the cohesive elements is also useful to prevent the interpenetration of the skin and stringer.

The force-displacement curves in Figure 11(a) represent the response of the six configurations taken into account. It can be observed that the initial axial stiffnesses for all configurations are identical since the stiffness is not influenced by the dimension of a pre-existing delamination. On the other hand, the collapse load, which is identified by the sudden drop of load, is reduced with increasing size of the pre-existing damage. The results shown in Figure 11(b) indicate that the collapse load decreases with a mostly linear behavior in the range of inserts sizes between 0 and 40 *mm*. The collapse load of the panel with the 40 *mm* insert is 12.8 *kN*, which is 55% of the load corresponding to the pristine panel. For pre-existing defects larger than 40 *mm*, the reduction in collapse load as a function of pre-existing damage is less significant because the skin buckles early and the stringer carries a greater portion of the load.

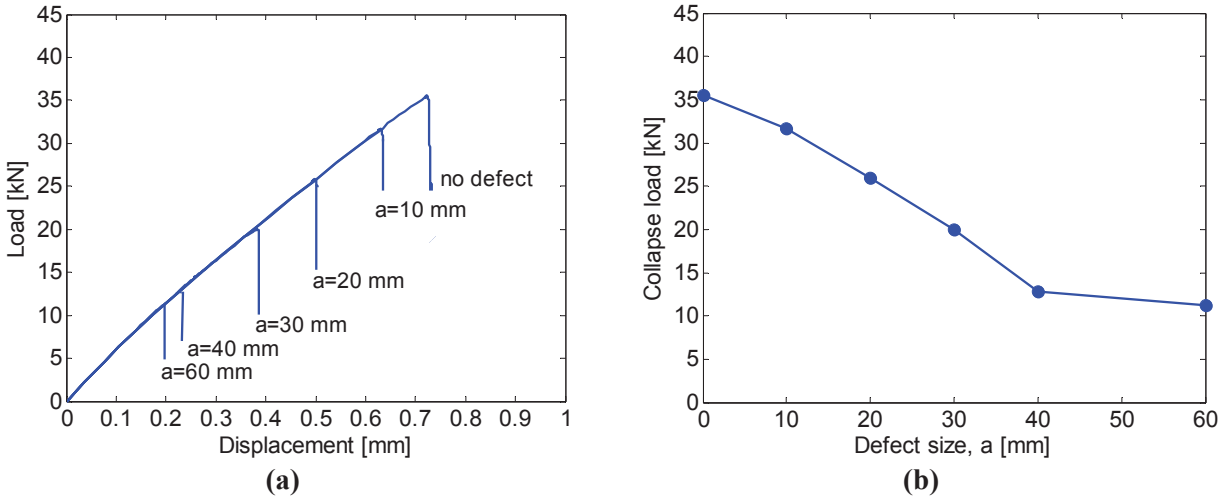

Figure 11. Effect of defect size: (a) force-displacement curve, (b) collapse load versus defect size.

The panels with 10 *mm* and 40 *mm* insert sizes are illustrated in Figures 12(a) and 12(d), respectively. The contour of the cohesive elements damage variable is shown for the panel with a 10 *mm* insert size in Figures 12(b) and 12(c), and for the panel with 40 *mm* insert size in Figures 12(e) and 12(f). The results are reported at the maximum load and after the maximum load for both configurations.

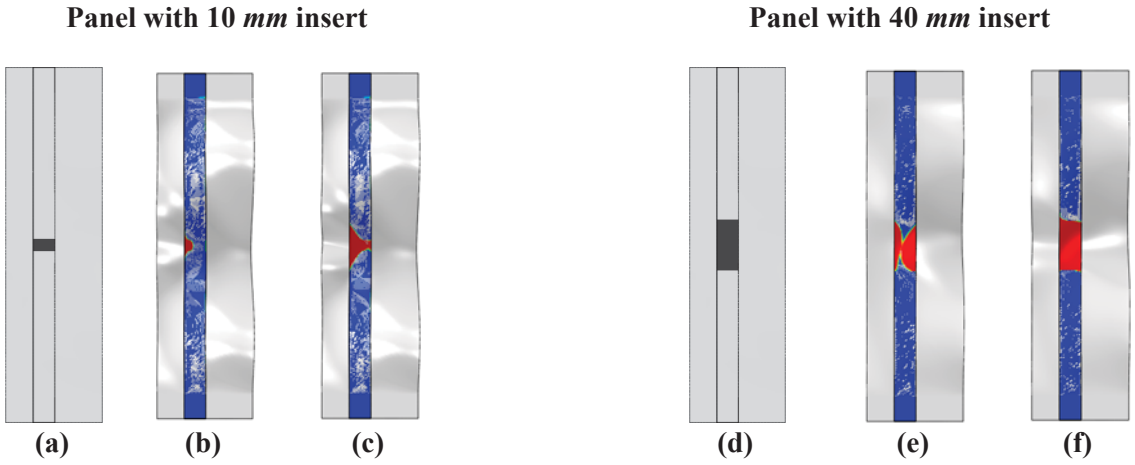

Figure 12. Panels with pre-existing bondline defect:
(a) and (d) pre-damaged area, (b) and (e) contour of cohesive element damage variable at maximum load, (c) and (f) contour of cohesive element damage variable after the maximum load.

The portion of structure on the left of the cohesive element layer is the skin under the stringer. The part on the right is the skin of the panel. It can be observed that different insert sizes determine different failure mechanisms. For the panel with a 10-*mm* damage of Figures 12(a) and 12(b), the separation between the skin and the stringer starts from the inside of the stringer to the outside, while for the panel with 40 *mm* the skin/stringer separation on both sides of the stringer flange since the beginning.

B. Virtual testing of a redesigned stringer

The use of the simplified model to perform design evaluations is illustrated in the following example. A concept for improving the panel collapse load can be extracted from an observation of the effect of the postbuckling deformation of the skin inside the stringer on the collapse mode. Consequently, it could be expected that the collapse load would be increased if the mode jumping of the skin under the stringer could be delayed.

The transition of the postbuckled deformed shape from one configuration to another is a complex nonlinear phenomenon. Although no closed-form solutions or simple design guidelines exist to quickly establish how it is possible to avoid or delay the mode jumping of a portion of structure, it can be expected that the mode transition of the skin inside the stringer would be delayed by narrowing the width of the stringer.

A design is proposed in which the width of the skin under the stringer is reduced from 42 *mm* to 26 *mm* by translating the stringer flange closer to the longitudinal line of symmetry of the panel, as shown in Figures 13(a) and 13(b). The total width of the panel and the amount of stringer material area are kept constant so that a comparison could be performed between equal-weight configurations. In particular, the height of the stringer is increased from 30 *mm* to 31.5 *mm*, and, to maintain a constant cross-section area, the web angle measured from the normal to the skin is reduced from 25° to 7.5°.

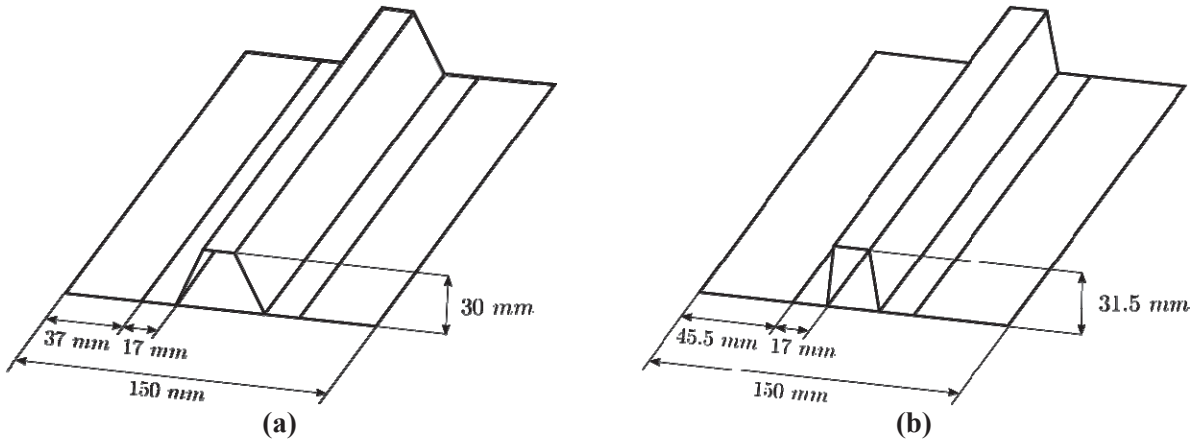

Figure 13. Panel configuration: (a) reference, (b) improved.

A comparison of the force-displacement results predicted for the two configurations is shown in Figure 14. The first portion of the curve shows that the prebuckling stiffness of both configurations is identical. Indeed, the two configurations possess the same cross-sectional area. On the other hand, the postbuckling response of the improved configuration presents a smaller stiffness compared to the reference configuration. This response is explained observing that the improved configuration is characterized by a wider portion of external skin, which is also the portion of structure involved in the first buckling of the panel and responsible for the loss of stiffness.

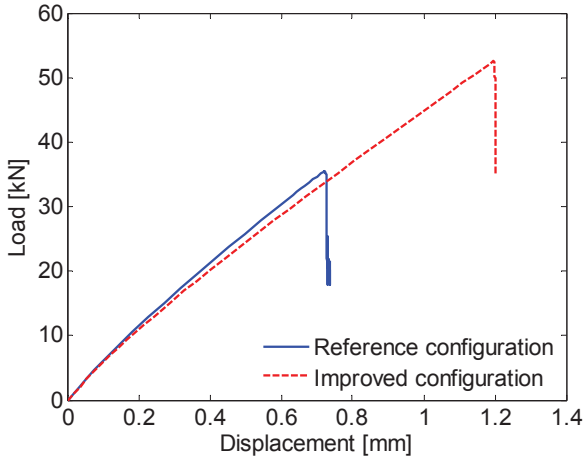

Figure 14. Force–displacement curves for reference and improved configurations.

It is interesting to observe that the collapse load of the improved configuration is 52.6 *kN*, or 32% higher than the reference configuration. The applied displacement at collapse is 1.2 *mm*.
The skin/stringer delamination of the improved design is illustrated in Figure 15, where the contour of the cohesive elements damage variable is shown.

Figure 15. Delamination on the improved configuration: (a) onset, (b) at maximum load.

Compared to the nominal design, the improved design is characterized by a different mechanism of delamination onset and growth. In particular, the delamination starts from the external part, as shown in Figure 15(a), and propagates to the internal part of the panel, as seen in Figure 15(b). This response is explained by the fact that no mode jumping is observed, as the narrowness of the stringer in the new design delays the mode jumping to load levels above the collapse load.

VII. Global/local approach

As was previously discussed, the SSC specimen is developed such that its postbuckling response, failure characteristics, and damage tolerance are similar to those of a corresponding multistringer panel subjected to compression loads. However, when complex loading or structural configurations must be considered, the assumption of periodicity becomes invalid and, consequently, the evaluation of the response and failure must be conducted on the full multistringer panel rather than on a smaller specimen.

A procedure is hereby proposed for assessing the damage tolerance of a postbuckled multistringer panel. In particular, the procedure provides a computationally efficient method to identify the critical strength and the critical areas of a multistringer panel.

A. Description of the approach

The analysis strategy consists of two main models: a global and a local model. First, the analysis of the entire panel is performed using a model with a relatively coarse mesh. This global model is composed exclusively of shell elements and is therefore unable to capture the onset and the propagation of delaminations. In addition, the material response is assumed to be linear elastic. Therefore, no convergence difficulties occur during the quasi-static load incrementation. The goal of the global analysis step is to determine the displacement field of the entire multistringer panel, which is used in the second step as a boundary condition for the local models.

In the second step, local analyses are performed using an SSCS-type model. The local models can be any small portion of the structure that the designer wants to analyze in detail. The local models are characterized by a high level of refinement. They are realized with shell elements, while cohesive elements are introduced between the skin and the stringer. The local models are loaded along the boundaries in displacement control using the results obtained from the global analysis. An interpolated displacement field based on the incremental solutions of the global model is generated automatically by the Abaqus *Submodel*[19] method. The local analyses are performed with an implicit dynamic step, which is an effective procedure to avoid the convergence issues related to the potential onset of delaminations.

Since the collapse of the panel is sudden and governed by the unstable growth of a delamination, the global and local analyses can be uncoupled until the onset of collapse. If the evolution of damage were to change appreciably the stiffness of the local model, then an iterative procedure to update the global model with the results obtained from the local analysis would be necessary.

B. Global and local models

The multistringer panel considered for the present study is shown in Figure 16. The panel has dimensions of 680 x 720 *mm* and it is longitudinally stiffened by five hat stringers. The area investigated using detailed local analyses consists of the central stringer. The local zone extends along the transverse direction to include half portion of the bay. The two external portions close to the loaded boundaries are excluded to avoid local effects. The resulting area of interest has a length 580 *mm* and a width equal to 152 *mm*. For efficiency, the local analysis is performed by dividing the area of interest into five smaller local models. In particular, the local models were selected to be 116-*mm* long, as illustrated in Figure 16(a) and identified by the numbers 1 to 5. In addition, the four overlapping models numbered 6-9 in Figure 16(b) were used to avoid potential boundary effects in the local models in cases where delaminations were to initiate near the edges of the local models. The overlap models are offset by 58 *mm* in the longitudinal direction with respect to models 1 to 5.

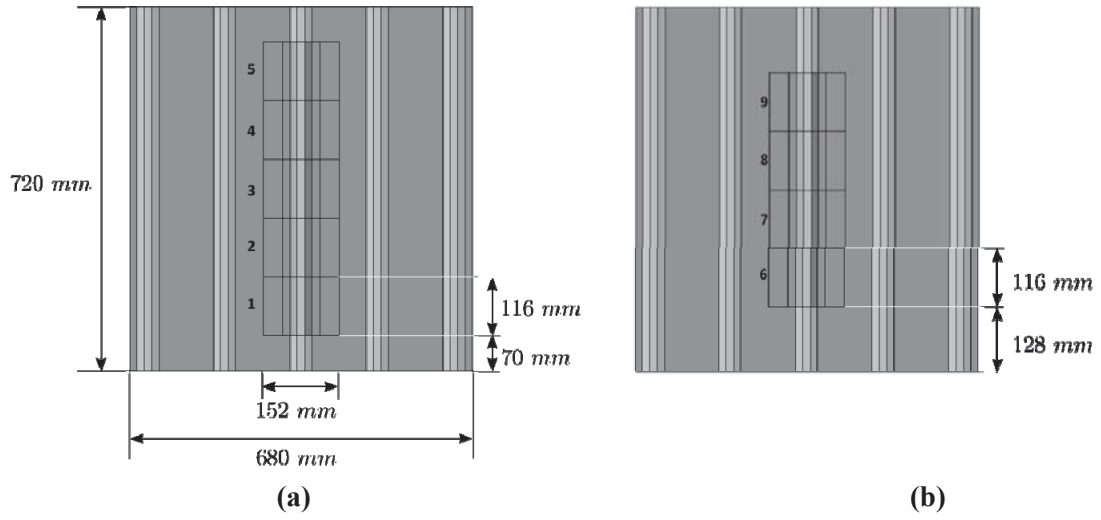

Figure 16. Local models and panel geometry: (a) local models 1 to 5, (b) overlap local models 6 to 9.

C. Results

The global/local procedure is conducted using a global model composed of shell elements with a typical mesh size of 5 x 5 *mm*. The total number of degrees of freedom is 171,390. Based on the analysis presented in the previous sections, the local model uses a typical mesh size of 1.0 x 1.0 *mm*. The corresponding number of degrees of freedom for each local model is 185,328.

The results of the global/local procedure are summarized in Figures 17 and 18. The out-of-plane deflection contours on the skin are shown on the global model for an applied end displacement of 2.50 *mm,* which corresponds to an applied strain of 0.35%. The hat-stringers are removed for visualization of the response in the portions of skin under the stringers. The results of the local models are reported in terms of the damage state of the cohesive elements at the corresponding maximum load. The critical areas are the ones exhibiting fully damaged cohesive elements, and the corresponding longitudinal positions on the global panel are identified by the dotted lines. The applied displacements at the failure of the local models are reported on the right columns of the figures.

The results indicate that delaminations can initiate as a consequence of two different postbuckling deformations modes. The first and most common delamination mode initiates on the inside edge of the stiffener flange and is induced by the splitting of a half-wave of the skin under the stringer. It can be observed in Figure 17, for instance, that the buckles for model 1 in the internal portion of the skin tend to pull away the skin from the stringer, and therefore represent a failure mechanism which is mainly governed by mode I. This delamination event was also observed in the SSCS and simplified models.

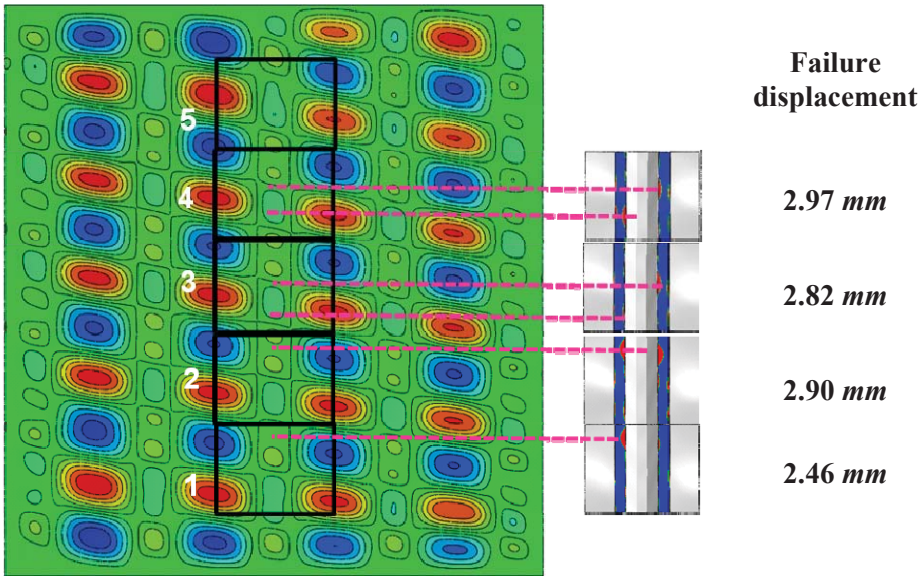

Figure 17. Results of global analysis and local models 1 to 5.

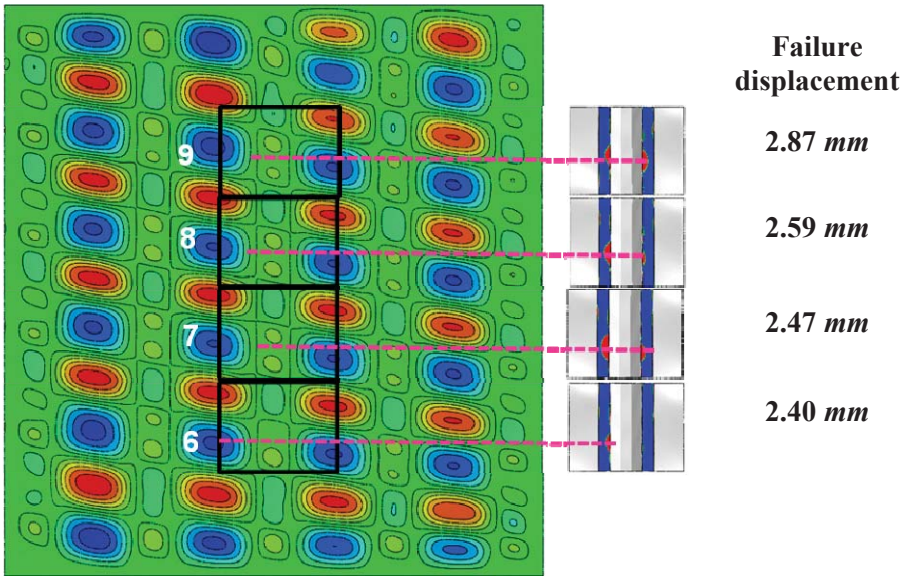

Figure 18. Results of global analysis and local models 6 to 9.

A second type of delamination can initiate at skin inflection points along the stringer flanges. This second mode of delamination has a stronger mode II component and it propagates at higher applied loads than the first mode of delamination.

It can also be noted from Figure 17 that displacement for collapse of the local model 2 (2.90 *mm*) is much higher than that of the local model 1 (2.46 *mm*), even though the modes of deformation appear to be similar. This difference can be explained by the fact that the delaminations predicted by model 2 are close to the boundaries of the local model. The influence of the boundary conditions is confirmed by the comparison with the local models 6 and 7, which cover the critical areas predicted by the models 1 and 2. However, the longitudinal position of the models 6 and 7 reduces the influence of the boundaries and

provides a more accurate description of the delamination onset and propagation. Indeed, the models 6 and 7 collapse at lower load levels that correspond to applied displacements of 2.40 *mm* and 2.47 *mm*, respectively, which are similar to that of model 1.
The critical displacements for models 3 and 4 are higher than those of models 1 and 2 and, therefore, they do not represent critical areas of a pristine stringer. However, it is interesting to observe that a different failure mechanism is exhibited in these local models compared to models 1 and 2. This behavior is clarified by the representation of the local model 4, which is reported in Figure 19. The contours of the out-of-plane displacements and the damage state of the cohesive elements are reported at the peak load, which corresponds to an applied displacement of 2.97 *mm*.

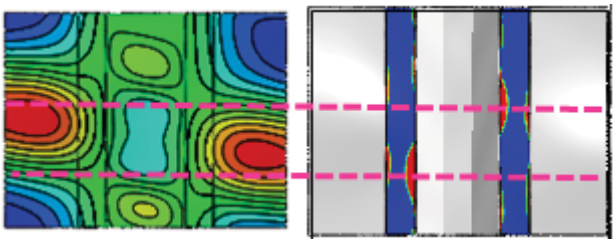

Figure 19. Results on model 4.

The deflected surface of Figure 19 displays two nodal lines in the skin outside the stringer, as highlighted by the two dotted lines. It can be observed that two delaminations develop at the nodal lines, and the failure mechanism is characterized by a significant mode II component.
The models 8 and 9 collapse at displacements of 2.59 and 2.87 *mm*, respectively, in the same mode I-dominated delamination as models 1 and 2, 6 and 7.
It is interesting to observe that the applied displacement corresponding to the collapse load of the local models increases from the bottom to the top of the panel. This effect is ascribed to the skewness of the buckled surface, which is due to the bending/twisting coupling induced by the lay-up stacking sequence.
It is interesting to observe the skew angle of the buckling pattern at different longitudinal positions. The skew angle is the angle of a line connecting the buckle crests of four adjacent bays. It can be observed in Figure 17 that the line passing through the crests of the lower section is approximately horizontal at the lower section, while it is characterized by a not zero skew angle at the upper section of the panel.
A comparison of the critical loads for local models 1 to 9 indicates that the weakest location along the central stringer is contained within local model 6. The critical displacement predicted by the global/local approach is 2.40 *mm*, which corresponds to a 0.33% strain. It is interesting to compare this result with the failure strain obtained from the SSCS analysis, and whose results are reported in Figure 7. The SSCS fails for an applied displacement of 0.89 *mm*, which corresponds to a 0.37% strain. The difference between the failure strain obtained with the global/local approach and the SSCS is 10%, so revealing the ability of the SSCS to reproduce the failure response of the multi-stiffened panel with a satisfactory level of accuracy.
In terms of computational times, the global analysis requires approximately 2 hours on a desktop workstation, while the local analysis requires approximately 3 hours. Consequently, the overall procedure can be carried out in a total time of 29 hours.

D. Mesh sensitivity

A comparison is presented between the local model 6, shown in Figure 20(a), and a model realized with a finer mesh of 0.5 *mm* and interlaminar strength equal to 50 *MPa*, reported in Figure 20(b). The goal is to verify that even the collapse load of the multistringer panel is not influenced by the interlaminar strength, and the use of the 1.0 *mm* mesh and σ_{zz} equal to 25 *MPa* is appropriate.

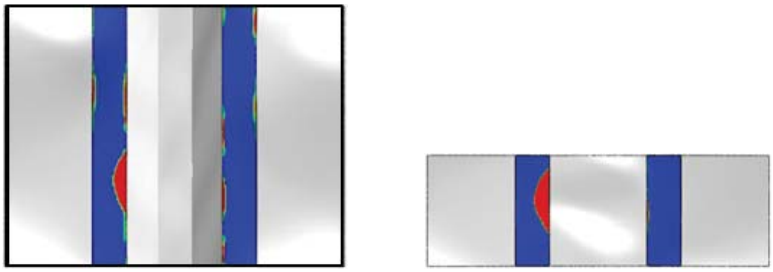

(a) **(b)**

Figure 20. Critical local model: (a) interlaminar strength 25 *MPa*, mesh 1.0 x 1.0 *mm*, (b) interlaminar strength 50 *MPa,* mesh 0.5 x 0.5 *mm*.

The comparison between Figures 20(a) and 20(b) reveals no differences in terms of delamination onset and propagation mechanism. Indeed, the contour of the damage variables of the cohesive elements of the two models is very similar. A slight difference is observed in terms of critical applied displacement, which increases from 2.40 *mm* to 2.54 *mm*.

The force displacement-curve of the multistringer panel is presented in Figure 21, together with the collapse loads calculated with the two different meshes.

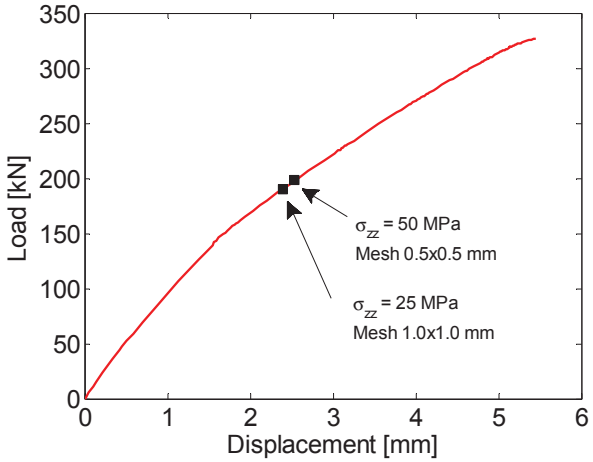

Figure 21. Comparison of predicted collapse loads using different mesh size.

The collapse load obtained with the 1.0 *mm* mesh is equal to 190.6 *kN*, while the more refined mesh of 0.5 *mm* determines a value of 198.0 *kN*. The two loads differ by less than 4%, showing that the 1.0 *mm* mesh with reduced interlaminar strength properties (25 *MPa*) allows an accurate prediction of the collapse laod.

VIII. Conclusions

A study of the response of postbuckled panels using models of different levels of approximation was conducted. A fast parametric finite element model was developed to gain insight into the structural postbuckling response, the initiation and propagation of delaminations, and their effect on the collapse load. The reduced computational time for this simplified model was also useful to conduct sensitivity studies on the effects of mesh refinement, material properties, defect dimensions, and stringer configuration. The results of the analyses indicate that the delamination-induced collapse of the stiffened panel investigated is geometrically driven. A postbuckling mode transition of the portion of skin between the two stringer webs was found to induce a mode I delamination of the stringer. The influence of different bond defect sizes on the collapse load was examined. In addition, the understanding of the mechanism of collapse extracted from the analyses was also used to develop an improved stringer design that constrains the mode transition for a higher collapse load. The computational efficiency of the simplified model developed in this study illustrates the ease with which such a parametric model can be used in a design environment.

Finally, a global/local methodology was presented to identify the weakest spots of the multistringer panel configuration loaded in compression. The procedure makes use of a relatively coarse global mesh of the panel in conjunction with a local model that relies on cohesive elements to capture the delamination failure modes. The multi-level methodology represents an efficient strategy to identify the weak spots and to predict the collapse load of postbuckled stiffened panels subjected to arbitrary loading conditions.

References

1. Abramovich, H., Weller, T., Bisagni, C., "Buckling Behavior of Composite Laminated Stiffened Panels under Combined Shear-Axial Compression," *Journal of Aircraft*, Vol. 45, No. 2, 2008, pp. 402–413.

2. Cordisco, P., Bisagni, C., "Cyclic Buckling Tests under Combined Loading on Predamaged Composite Stiffened Boxes," *AIAA Journal*, Vol. 49, No. 8, 2011, pp. 1795-1807.

3. Greenhalgh, E., Meeks, C., Clarke, A., Thatcher, J., "The Effect of Defects on the Performance of Post-Buckled CFRP Stringer-Stiffened Panels," *Composites Part A: Applied Science and Manufacturing*, Vol. 34, No. 7, 2003, pp. 623–633.

4. Zimmermann, R., Klein, H., Kling, A., "Buckling and Postbuckling of Stringer Stiffened Fibre Composite Curved Panels - Tests and Computations," *Composite Structures*, Vol. 73, No. 2, 2006, pp. 150–161.

5. Taki, T., Kitagawa, T., "Post-Buckling Strength of Composite Stiffened Panel under Shear Load," *1st AIAA Aircraft Engineering, Technology, and Operations Congress*, AIAA Paper 95-393, September 1995.

6. Cosentino, E., Weaver, P.M., "Approximate Nonlinear Analysis Method for Debonding of Skin/Stringer Composite Assemblies," *AIAA Journal*, Vol. 46, No. 5, 2008, pp. 1144-1159.

7. Ambur, D.R., Jaunky, N., Dávila, C.G., Hilburger, M.W., "Progressive Failure Studies of Composite Panels with and without Cutouts," *NASA/CR-2001-211223,* ICASE Report No. 2001-27, 2001.

8. Basu, S., Waas, A.M., Ambur, D.R., "Prediction of Progressive Failure in Multidirectional Composite Laminated Panels," *International Journal of Solids and Structures*, Vol. 44, No. 9, 2007, pp. 2648-2676.

9. Maimí, P., Camanho, P.P., Mayugo, J.A., Dávila, C.G., "A Continuum Damage Model for Composite Laminates: Part I - Constitutive Model," *Mechanics of Materials*, Vol. 39, No. 10, 2007, pp. 897-908.

10. Maimí, P., Camanho, P.P., Mayugo, J.A., Dávila, C.G., "A Continuum Damage Model for Composite Laminates: Part II - Computational Implementation," *Mechanics of Materials*, Vol. 39, No. 10, 2007, pp. 909-919.

11. Krueger, R., "The Virtual Crack Closure Technique: History, Approach and Applications," *NASA/CR-2002-211628,* ICASE Report No. 2002-10, 2002.

12. Camanho, P.P., Dávila, C.G., de Moura, M.F.S.F., "Numerical Simulation of Mixed-Mode Progressive Delamination in Composite Materials," *Journal of Composite Materials*, Vol. 37, No. 16, 2003, pp. 1415-1438.

13. Dávila, G.C., Camanho, P.P., Turon, A., "Effective Simulation of Delamination in Aeronautical Structures Using Shells and Cohesive Elements," *Journal of Aircraft*, Vol. 45, No. 2, 2008, pp. 663-672.

14. Moës, N., Dolbow, J., Belytschko, T., "A Finite Element Method for Crack Growth without Remeshing," *International Journal for Numerical Methods in Engineering*, Vol. 46, No. 1, 1999, pp. 131-150.

15. Orifici, A.C., Thomson, R.S., Degenhardt, R., Bisagni, C., Bayandor, J., "A Finite Element Methodology for Analysing Degradation and Collapse in Postbuckling Composite Aerospace Structures," *Mechanics of Composite Materials*, Vol. 43, No. 1, 2007, pp. 9-28.

16. Bertolini, J., Castanié, B., Barrau, J.J., Navarro, J.P., Petiot, C. "Multi-Level Experimental and Numerical Analysis of Composite Stiffener Debonding. Part 2: Element and Panel Level," *Composite Structures*, Vol. 90, No. 4, 2009, pp. 392-403.

17. Benzeggagh, M.L., Kenane, M., "Measurement of Mixed-Mode Delamination Fracture Toughness if Unidirectional Glass/Epoxy Composites with Mixed-Mode Bending Apparatus," *Composite Science and Technology,* Vol. 56, No. 4, 1996, pp. 439-449.

18. Bisagni, C., Vescovini, R., Dávila, C.G., "Single-Stringer Compression Specimen for the Assessment of Damage Tolerance of Postbuckled Structures," *Journal of Aircraft*, Vol. 48, No. 2, 2011, pp. 495-502.

19. Abaqus 6.10 User's Manual, Dassault Systèmes, Providence, RI, USA, 2010.

20. Camanho, P.P., Maimí, P., Dávila, C.G., "Prediction of Size Effects in Notched Laminates Using Continuum Damage Mechanics," *Composites Science and Technology*, Vol. 67, No. 13, 2007, pp. 2715-2727.

21. Dávila, C.G., Rose, C.A., Camanho, P.P., "A Procedure for Superposing Linear Cohesive Laws to Represent Multiple Damage Mechanisms in the Fracture of Composites," *International Journal of Fracture,* Vol. 158, No. 2, 2009, pp. 211-223.

22. Schön, J., Nyman, T., Blom, A., Ansell, H., "A Numerical and Experimental Investigation of Delamination Behaviour in the DCB Specimen," *Composites Science and Technology*, Vol. 60, No. 2, 2000, pp. 173-184.

23. Pereira, A.B., de Morais, A.B., "Mode I Interlaminar Fracture of Carbon/Epoxy Multidirectional Laminates," *Composites Science and Technology*, Vol. 64, No. 13-14, 2004, pp. 2261-2270.

REPORT DOCUMENTATION PAGE

Form Approved
OMB No. 0704-0188

1. REPORT DATE *(DD-MM-YYYY)*	2. REPORT TYPE	3. DATES COVERED *(From - To)*
01- 02 - 2012	Technical Memorandum	

4. TITLE AND SUBTITLE

Simplified Models for the Study of Postbuckled Hat-Stiffened Composite Panels

5a. CONTRACT NUMBER

5b. GRANT NUMBER

5c. PROGRAM ELEMENT NUMBER

6. AUTHOR(S)

Vescovini, Riccardo; Davila, Carlos G.; Bisagni, Chiara

5d. PROJECT NUMBER

5e. TASK NUMBER

5f. WORK UNIT NUMBER

284848.02.04.07.01

7. PERFORMING ORGANIZATION NAME(S) AND ADDRESS(ES)

NASA Langley Research Center
Hampton, VA 23681-2199

8. PERFORMING ORGANIZATION REPORT NUMBER

L-20118

9. SPONSORING/MONITORING AGENCY NAME(S) AND ADDRESS(ES)

National Aeronautics and Space Administration
Washington, DC 20546-0001

10. SPONSOR/MONITOR'S ACRONYM(S)

NASA

11. SPONSOR/MONITOR'S REPORT NUMBER(S)

NASA/TM-2012-217336

12. DISTRIBUTION/AVAILABILITY STATEMENT

Unclassified - Unlimited
Subject Category 24
Availability: NASA CASI (443) 757-5802

13. SUPPLEMENTARY NOTES

14. ABSTRACT

The postbuckling response and failure of multistringer stiffened panels is analyzed using models with three levels of approximation. The first model uses a relatively coarse mesh to capture the global postbuckling response of a five-stringer panel. The second model can predict the nonlinear response as well as the debonding and crippling failure mechanisms in a single stringer compression specimen (SSCS). The third model consists of a simplified version of the SSCS that is designed to minimize the computational effort. The simplified model is well-suited to perform sensitivity analyses for studying the phenomena that lead to structural collapse. In particular, the simplified model is used to obtain a deeper understanding of the role played by geometric and material modeling parameters such as mesh size, inter-laminar strength, fracture toughness, and fracture mode mixity. Finally, a global/local damage analysis method is proposed in which a detailed local model is used to scan the global model to identify the locations that are most critical for damage tolerance.

15. SUBJECT TERMS

Cohesive elements; Composites; Delamination; Fracture; Material characterization

16. SECURITY CLASSIFICATION OF:			17. LIMITATION OF ABSTRACT	18. NUMBER OF PAGES	19a. NAME OF RESPONSIBLE PERSON
a. REPORT	b. ABSTRACT	c. THIS PAGE			STI Help Desk (email: help@sti.nasa.gov)
					19b. TELEPHONE NUMBER *(Include area code)*
U	U	U	UU	30	(443) 757-5802